Journal of Great Lakes Research 46 (2020) 703–717

Contents lists available at ScienceDirect

Journal of Great Lakes Research

journal homepage: www.elsevier.com/locate/ijglr

What makes an elongated lake 'large'? Scales from wind-driven steady circulation on a rotating Earth

Marina Amadori [a,*], Sebastiano Piccolroaz [b], Henk A. Dijkstra [b], Marco Toffolon [a]

[a] Department of Civil, Environmental and Mechanical Engineering (DICAM), University of Trento, Trento, Italy
[b] Institute for Marine and Atmospheric Research Utrecht (IMAU), Department of Physics, Utrecht University, Utrecht, The Netherlands

ARTICLE INFO

Article history:
Received 10 May 2019
Accepted 17 October 2019
Available online 25 December 2019
Communicated by Jordi Prats

Keywords:
Ekman theory
Coriolis acceleration
Analytical solutions
Numerical modeling
Narrow lakes

ABSTRACT

When investigating wind-induced steady circulation, the effect of the acceleration due to Earth's rotation is often neglected in narrow lakes, but the argument behind this assumption is blurred. Commonly, when the horizontal dimension is smaller than the Rossby radius, the Coriolis force is considered unimportant, but this is correct only for inertial currents and barotropic and baroclinic waves. In this work, we revisit the classical Ekman transport solution for wind stress acting along the main axis of an elongated lake in steady-state conditions. We demonstrate that a secondary circulation develops and that the resulting crosswise volume transport, constrained in the closed domain, produces downwelling and upwelling that cannot be predicted by the standard Ekman formulas. We claim that the Rossby radius does not play any role in this process, which on the contrary is governed by the ratio between the actual depth and the thickness of the Ekman layer. The theoretical analysis is supported by numerical experiments to show the dependence on latitude, width, depth and turbulence closure.

Introduction

The role of Earth's rotation on three-dimensional circulation in an ocean is a rather classical subject after the seminal contribution by Vagn Walfrid Ekman at the beginning of the twentieth century (Ekman, 1905). Assuming steady and uniform conditions in a horizontally infinite water body, he derived an analytical solution for the vertical distribution of the horizontal velocity induced by the wind stress at the surface. Ekman found that the resulting volume transport is oriented perpendicular to the wind stress, a simple observation with profound consequences. His solution was further extended to more complex conditions by the oceanographic community (see Appendix A for an exhaustive literature review), but few contributions focused on the quantification of the transport in closed water bodies such as lakes.

When investigating the circulation in enclosed or semi-enclosed basins, the inclusion/exclusion of the Earth's rotation as a relevant process often produces some ambiguity. It is a common assumption in limnological studies that Earth's rotation is relevant only in 'large' water bodies, while it can be neglected in relatively 'small' ones. The origin of this assumption is twofold: first, it comes from the literature on gravity waves and density-driven currents in rotating water bodies, where the horizontal extent of the basin is compared to the Rossby radius. Secondly, it comes from the fact that the Ekman problem was initially designed for the case of infinitely wide ocean, far enough from boundaries.

On the first point, there are a number of situations where the relevance of Earth's rotation can be assessed referring to the Rossby number,

$$\mathrm{Ro} = \frac{R}{L}, \tag{1}$$

with R being the Rossby radius and L the characteristic horizontal size. The Rossby radius is often computed as $R = U/f$, where U is a typical scale of flow velocity and $f = 2\Omega \sin\phi$ the Coriolis parameter, with Ω the angular frequency and ϕ the latitude on Earth. A different definition of Ro is based on the so-called Rossby radius of deformation, $\tilde{R} = c/f$, where $c = \sqrt{gH}$ is the celerity of the barotropic wave, with g the gravitational acceleration and H the depth (Rossby, 1937). If baroclinic waves are considered, $c = \sqrt{g' H_1 H_2 / H}$, with g' the reduced gravity in stratified conditions and H_1 and H_2 the thicknesses of a two-layer stratification, such that $H = H_1 + H_2$ (Rossby, 1938). Based on the traditional scaling analysis, water bodies smaller than R (i.e., $\mathrm{Ro} > 1$) are not significantly affected by rotation, and the Coriolis acceleration is considered important only if $\mathrm{Ro} < 1$ (Gill, 1982). Such a scaling, which was formulated for oscillatory motions induced by the Earth's

* Corresponding author.
E-mail address: marina.amadori@unitn.it (M. Amadori).

https://doi.org/10.1016/j.jglr.2019.10.013
0380-1330/

rotation, was next extended to basin-scale circulation and vertical current structure in lakes (Hutter et al., 1991; Rueda and Vidal, 2009). In this respect, we note that the existence of different definitions of the Rossby number, which depend on the phenomenon under investigation, may generate some confusion.

Concerning the second point, i.e. the legacy of the original formulation of the Ekman problem in an infinite domain (Ekman, 1905), several generalizations of the theory have been proposed to describe the effect of Earth's rotation on steady circulation in enclosed or semi-enclosed basins, with relevant contributions in the field of estuarine and coastal oceanography (see Appendix A). In several of these contributions, the so-called Ekman depth

$$D_E = \sqrt{\frac{2\nu_z}{f}} \tag{2}$$

is introduced as the relevant scale, with ν_z a reference value of the vertical viscosity, and the Ekman number, i.e. the ratio $\mathrm{Ek} = H/D_E$, enters into several analytical solutions. It is argued (Kasai et al., 2000) that, when Ek is small (i.e., $H \ll D_E$), the whole water column is inside the Ekman layer and the flow is governed by viscosity; when Ek is large ($H \gg D_E$), the effect of Coriolis force becomes important.

Hence, two different dimensional parameters seem to describe the role of Earth's rotation on steady circulation in closed domains. One of them (Ro) depends on the horizontal scales and the other one (Ek) on the vertical scales. The question arises as to what makes a lake 'large', such that we should include the Coriolis acceleration when investigating steady circulation? The answer to this relevant question is not clear-cut. In this paper, we tackle this question by deriving a simple analytical solution to interpret lake steady circulation dynamics for all latitudes and a wide range of lake sizes. The analytical solution is compared with numerical results to demonstrate its consistency and to investigate the role of some specific aspects such as the horizontal and vertical size of the basin, the bottom boundary condition, the turbulence model and the turbulence anisotropy on the resulting steady circulation.

Analytical solution

Mathematical formulation

In our analytical solution we assume an idealized rectangular domain of elongated shape characterized by length L along the main longitudinal axis (y), width B along the crosswise axis (x), and depth H along the vertical axis (z). The Cartesian reference system is centered in the middle of the lake surface (Fig. 1), with the z-axis pointing upward.

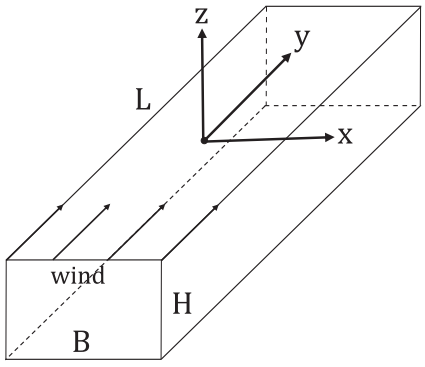

Fig. 1. Sketch of the simplified domain and wind forcing directed along the longitudinal axis of the lake.

We describe the flow with the Reynolds-averaged Navier Stokes equations in hydrostatic approximation (3)–(6), for a fluid of uniform density,

$$\frac{\partial u}{\partial t} + u\frac{\partial u}{\partial x} + v\frac{\partial u}{\partial y} + w\frac{\partial u}{\partial z} = fv - \frac{1}{\rho}\frac{\partial p}{\partial x} + \frac{\partial}{\partial x}\left(\nu_h\frac{\partial u}{\partial x}\right) + \frac{\partial}{\partial y}\left(\nu_h\frac{\partial u}{\partial y}\right) + \frac{\partial}{\partial z}\left(\nu_z\frac{\partial u}{\partial z}\right), \tag{3}$$

$$\frac{\partial v}{\partial t} + u\frac{\partial v}{\partial x} + v\frac{\partial v}{\partial y} + w\frac{\partial v}{\partial z} = -fu - \frac{1}{\rho}\frac{\partial p}{\partial y} + \frac{\partial}{\partial x}\left(\nu_h\frac{\partial v}{\partial x}\right) + \frac{\partial}{\partial y}\left(\nu_h\frac{\partial v}{\partial y}\right) + \frac{\partial}{\partial z}\left(\nu_z\frac{\partial v}{\partial z}\right), \tag{4}$$

$$\frac{1}{\rho}\frac{\partial p}{\partial z} + g = 0, \tag{5}$$

$$\frac{\partial u}{\partial x} + \frac{\partial v}{\partial y} + \frac{\partial w}{\partial z} = 0, \tag{6}$$

where u, v and w are the three components of the velocity vector, t is time, p is pressure, and g is the acceleration due to gravity. The Reynolds stresses were closed using the Boussinesq formulation, where the eddy viscosity tensor is assumed anisotropic, with the vertical ν_z smaller than the horizontal ν_h. Following the standard derivation originally proposed by Ekman (1905), we consider a steady state with constant in time and uniform in space eddy viscosities. While Ekman neglected the pressure gradient, we retain it following more elaborate solutions that take into account the effect of geostrophic gradients (e.g., Welander, 1957). In the original formulation of the Ekman problem for an unbounded domain, horizontal gradients of velocity were neglected and all the non-linear advection terms, as well as horizontal diffusion terms, vanished giving a linearized version of the RANS. Following this simplification, standard solutions extended the linearized equations of motion also to the case of closed domains (Hutter et al., 2011; Simons, 1980). However, we note that in presence of lateral boundaries, the assumption of horizontal uniformity is not necessarily valid and must be verified. Toffolon and Rizzi (2009) demonstrated via a dimensional scaling that longitudinal gradients can be neglected in the central trunk of non-rotating elongated lakes, while Toffolon (2013) showed that in the rotating case also the crosswise gradients are negligible as a first approximation on condition that we focus on the central part of the cross section. Under such an approximation we simplify Eqs. (3), (4) and (6) removing the non-linear advective and diffusive terms depending on horizontal gradients of velocity. As a consequence, in the central part of the domain the continuity equation reduces to $\frac{\partial w}{\partial z} = 0$, which gives $w = 0$ under a rigid lid approximation. As a result of these assumptions, also the non-linear advective terms and $w\frac{\partial u}{\partial z}$ disappear and the problem to be solved reduces to a system of two linear equations depending only on the vertical direction and on the two components of the slope of the free surface z_t:

$$\nu_z\frac{\partial^2 u}{\partial z^2} + fv = g\frac{\partial z_t}{\partial x}, \tag{7}$$

$$\nu_z\frac{\partial^2 v}{\partial z^2} - fu = g\frac{\partial z_t}{\partial y}, \tag{8}$$

The originally three-dimensional problem is simplified into a one-dimensional (1D) problem of momentum transfer along the vertical direction z from the surface to the bottom (left-hand side of the equations), with the barotropic pressure gradients on the right-hand side to be determined. The first problem alone is nothing but the traditional vertical Ekman problem, where friction determi-

nes the vertical distribution of momentum to balance the Coriolis acceleration and is independent of the lateral walls. The second problem interacts with the horizontal boundaries of the domain, whose presence provides the relations needed to determine the value of barotropic pressure gradients.

The two second-order differential equations are complemented with suitable boundary conditions. Referring again to standard solutions, here we assume uniform wind stress at the surface ($z = z_t$),

$$\frac{\partial u}{\partial z}\Big|_{z=z_t} = \frac{\tau_x}{\rho \nu_z}, \qquad \frac{\partial v}{\partial z}\Big|_{z=z_t} = \frac{\tau_y}{\rho \nu_z}, \tag{9}$$

and no-slip condition at the bottom ($z = z_b$),

$$u|_{z=z_b} = 0, \qquad v|_{z=z_b} = 0. \tag{10}$$

In Eq. (9), τ_x and τ_y are the two components of wind tangential stress $\boldsymbol{\tau} = (\tau_x, \tau_y)$, where $\boldsymbol{\tau} = \rho_a C_d |\mathbf{U_w}| \mathbf{U_w}$, ρ_a is the air density, C_d the drag coefficient, and $\mathbf{U_w}$ is the wind velocity vector at 10 m above the water surface. An alternative solution can be obtained by changing the bottom boundary condition: the case of free-slip (vanishing shear stress) at the bottom is discussed in Appendix B.

The differential problem composed by (7), (8) with boundary conditions (9) and (10) is mathematically closed if the surface slope $(\partial z_t/\partial x, \partial z_t/\partial y)$ is provided. The original solution neglected it due to the assumption of infinite domain (Ekman, 1905), while following contributions imposed it in the form of external geostrophic pressure gradients (Welander, 1957).

In our approach, we do not assume any external value of the surface slope, but we compute the value that satisfies the condition of vanishing volume transport across any surface separating the closed domain in two parts in the steady state. A similar condition was applied by Simons (1980) solely along the crosswise direction for the case of narrow and elongated basins, by Heaps and Hutter (1984) along the longitudinal in the non-rotating case and by Kasai et al. (2000) in both directions by assuming a net volume transport ($m^3\ s^{-1}$) along or across a cross section in a semi-enclosed basin. Here we assume that such net volume is zero (i.e., a limit case of the solution proposed by Kasai et al. (2000)), as a direct consequence of the presence of closed boundaries when the free surface does not change in time: the volume of any region of the domain cannot change and the incoming transport must be balanced by the outgoing one (Toffolon and Rizzi, 2009). Focusing again on the central part of the domain, we simplify this condition by assuming a local integral condition:

$$\int_{z_b}^{z_t} u\, dz = 0, \qquad \int_{z_b}^{z_t} v\, dz = 0. \tag{11}$$

Derivation of the solution

Introducing the complex variable $W = u + i\,v$, the problem composed by Eqs. (7)–(11) can be cast in a more compact form:

$$\nu_z \frac{\partial^2 W}{\partial z^2} - i f W = g S, \tag{12}$$

$$\frac{\partial W}{\partial z}\Big|_{z=z_t} = \frac{T}{\rho \nu_z}, \qquad W|_{z=z_b} = 0, \tag{13}$$

$$\int_{z_b}^{z_t} W\, dz = 0, \tag{14}$$

where $T = \tau_x + i\,\tau_y$ and $S = \partial z_t/\partial x + i\,\partial z_t/\partial y$.

To formulate the problem (12)–(14) in dimensionless form, we introduce:

$$\mathcal{T} = \frac{T}{T_0}, \qquad \omega = \frac{W}{U_0}, \qquad \sigma = \frac{S}{S_0}, \tag{15}$$

with the scales

$$T_0 = \sqrt{\tau_x^2 + \tau_y^2}, \qquad U_0 = \frac{T_0 H}{\rho \nu_z}, \qquad S_0 = \frac{T_0}{\rho g H}. \tag{16}$$

Finally, we introduce a boundary-fitted vertical coordinate

$$\zeta = \frac{z_t - z}{H}, \tag{17}$$

where $H = z_t - z_b$. We note that the axis ζ is directed downward (while z is pointing upwards), with $\zeta = 0$ at the surface and $\zeta = 1$ at the bottom, following a common notation (e.g., Hutter et al., 2011).

As a result, the dimensionless form of the problem (12)–(14) becomes

$$\frac{\partial^2 \omega}{\partial \zeta^2} - i\varepsilon^2 \omega = \sigma, \tag{18}$$

$$\frac{\partial \omega}{\partial \zeta}\Big|_{\zeta=0} = -\mathcal{T}, \qquad \omega|_{\zeta=1} = 0, \tag{19}$$

$$\int_0^1 \omega\, d\zeta = 0, \tag{20}$$

where the single dimensionless parameter

$$\varepsilon = \sqrt{\frac{f H^2}{\nu_z}} = \sqrt{2}\,\mathrm{Ek} \tag{21}$$

governs the problem ($\mathcal{T}$ indicates the wind direction only, so that $|\mathcal{T}| = 1$).

The two complex numbers obtained as integration constants from the integration of (18) can be determined using the two boundary conditions (19) if the value of σ is prescribed. This is the case of the traditional Ekman solution, whereby $\sigma = 0$, or when the surface slope is determined from a geostrophic balance (Simons, 1980). For a flow determined solely by wind set-up of the water level (excluding any rotational effect) and no-slip conditions at the bottom, $\sigma = 3/2\,\mathcal{T}$ and the free surface is tilted in the direction of the wind (e.g., Heaps and Hutter, 1984; Toffolon, 2013).

The general solution to the dimensionless problem (18,19) can be written as a function of σ (whatever prescribed or solved) and ε as follows:

$$\omega(\zeta) = \frac{\sin\left[\Theta(\zeta - 1)\right]}{\Theta \cos\Theta}\,\mathcal{T} + \left[\frac{1 - \cos(\Theta\zeta)}{\cos\Theta}\right]\frac{\sigma}{\Theta^2}, \tag{22}$$

where $\Theta = \frac{\sqrt{2}}{2}\varepsilon(1 - i)$ and, hence, $\varepsilon^2 = i\Theta^2$. As it is clear from Eq. (22), the solution is explicitly dependent on the free surface inclination expressed by the parameter σ.

In the case of closed lakes in steady conditions, Eq. (20) applies and forces the value of σ to respect the requirement of vanishing volume transport as

$$\sigma = \mathcal{T}\,\Theta\,\frac{1 - \cos\Theta}{\sin\Theta - \Theta\cos\Theta}. \tag{23}$$

From now on, the proposed solution, characterized by the integral condition valid for a closed boundary case, will be referred to as A2019. Hereafter, we refer to a wind aligned with the main axis of the lake ($\mathcal{T} = i$), such that the longitudinal y direction is also the along-wind direction and the imaginary part of the complex variables, while the crosswise x is the across-wind direction and the real part of the complex variables.

The behavior of the real (σ_x) and imaginary (σ_y) part of σ is represented in Fig. 2 as a function of ε. It immediately appears that the longitudinal components σ_y (Fig. 2a) ranges from 1 to 3/2 with a trend that is consistent with Simons (1980) in the case of narrow and elongated basins. In the crosswise direction, the surface slope σ_x (Fig. 2b) vanishes at the extremes of the ε range and has a bell shape suggesting that rotation plays a role on the crosswise component only in an intermediate range of H, f and ν_z.

The behavior of the surface velocity obtained from Eq. (22) by imposing $\zeta = 0$ is plotted in Fig. 3 and compared with the Ekman solution (E1905) in the finite-depth version. The longitudinal velocity ω_y (i.e. the imaginary part of the complex dimensionless velocity ω) is not affected by the Coriolis force for $\varepsilon < 1$ (Fig. 3a), while it starts being decelerated in favor of the crosswise flow ω_x for higher values of ε (Fig. 3b). In the range of ε where ω_x increases, ω_y decreases until the same magnitude is reached and the surface water moves at 45° to the right of the wind (Fig. 3c) as in the Ekman spiral theory. It is easily understood that the classical Ekman approach correctly describes the motion for large values of ε (deep lakes, high latitudes and/or weak mixing regimes), but it overestimates the velocity in both directions within the range of lower ε.

Limiting cases

Two limiting cases can be conveniently analyzed depending on the value of ε. First, we consider the case of very shallow lakes, where the shallowness is defined with respect to the Ekman depth ($H \ll D_E$). Note that D_E can become very large for vanishing values of f, for instance close to the equator where the influence of Coriolis acceleration disappears. For $\varepsilon \to 0$ (hence, $\Theta \to 0$), the solution (22) tends to

$$\omega(\zeta) = \mathcal{T}(1-\zeta) + \frac{\sigma}{2}(\zeta^2 - 1), \tag{24}$$

and the slope $\sigma = 3/2\mathcal{T}$ can be obtained from Eq. (23), revealing that the tilt of the free surface is exactly oriented as the wind forcing (see also Fig. 2 for low ε). Combining the two results, it is straightforward to obtain the well-known velocity profile induced by wind stress in a non-rotating system (e.g., Heaps and Hutter, 1984):

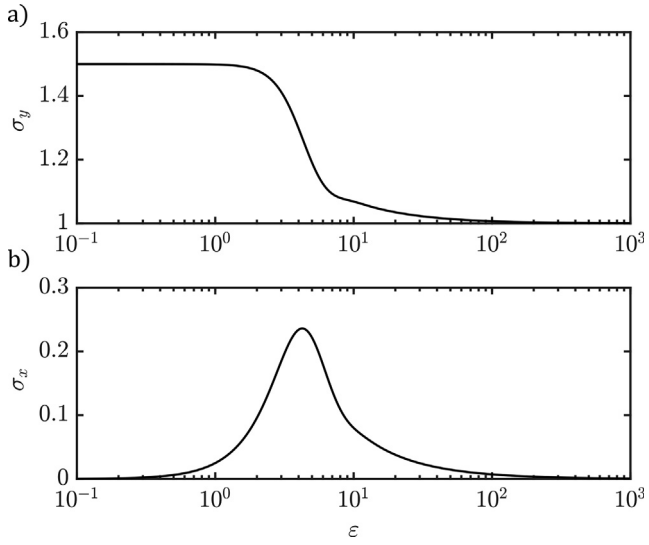

Fig. 2. Surface slope rescaled with the reference values S_0 from A2019 analytical solution: (a) longitudinal component σ_y, and (b) crosswise component σ_x. Wind aligned with the y axis, no-slip bottom boundary condition.

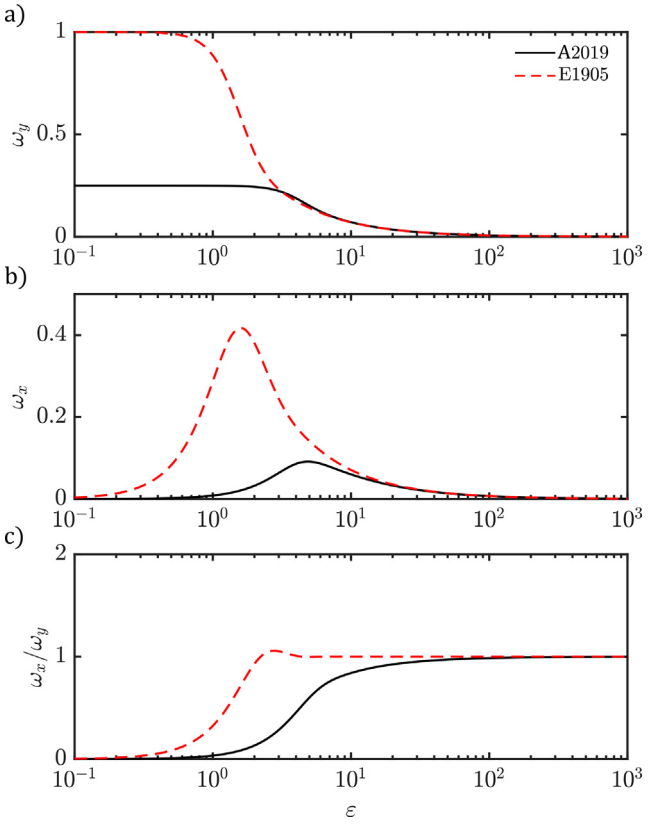

Fig. 3. Dimensionless surface velocity obtained from the analytical solutions A2019 and E1905: (a) longitudinal component ω_y , (b) crosswise component ω_x, and (c) direction. Wind aligned with the y axis, no-slip bottom boundary condition.

$$\frac{\omega}{\mathcal{T}} = \frac{1}{4} - \zeta + \frac{3}{4}\zeta^2. \tag{25}$$

It is interesting to analyze how the solution in the shallow case is modified by the Coriolis acceleration and how the correction depends on ε. By developing the solution (22) and (23) in Taylor series for $\varepsilon \ll 1$, we obtain that

$$\frac{\sigma}{\mathcal{T}} = \frac{3}{2} - \frac{i}{40}\varepsilon^2 + O(\varepsilon^4), \tag{26}$$

$$\frac{\omega}{\mathcal{T}} = \frac{1}{4} - \zeta + \frac{3}{4}\zeta^2 - \frac{i}{240}(1-\zeta)(2 + 2\zeta - 25\zeta^2 + 15\zeta^3)\,\varepsilon^2 + O(\varepsilon^4). \tag{27}$$

Eq. (26) shows that the longitudinal slope is not modified up to $O(\varepsilon^4)$, and that Coriolis acceleration produces a crosswise tilt at $O(\varepsilon^2)$. This is reflected in the velocity distribution of Eq. (27), where a secondary circulation develops without interfering with the primary flow, as already proposed by Toffolon (2013).

The second case is that of infinite depth ($\varepsilon \to \infty$). In this case, it is possible to demonstrate that $\sigma \to \mathcal{T}$ (see Fig. 2 for high ε). From a physical point of view, the consequence is that the actual slope, $S = S_0\sigma$, vanishes because $S_0 \to 0$ for $H \to \infty$ (see Eqs. (15) and (16)). Such a consideration suggests that the infinite-depth case tends to the traditional Ekman solution. In fact, the difference between the solution (22)–(23) and that obtained for $\sigma = 0$ becomes negligible for large values of ε.

Crosswise transport

We have seen that the A2019 solution (22,23) describes a flow field that is affected by the action of Coriolis acceleration (Fig. 3).

For small values of ε, a secondary motion is established without significantly altering the main flow (Toffolon, 2013). When ε grows, the longitudinal primary circulation is progressively modified and the crosswise velocity is enhanced until a state is reached where ω_x and ω_y are of the same magnitude (Ekman spiral).

In a closed water body, the crosswise transport produces a downwelling at the coast on the right of the wind (in the northern hemisphere) and upwelling at the leftward coast. It is therefore important to compute the crosswise flux by integrating the crosswise velocity profile from the surface to the depth where the velocity changes sign. Defining this point as z_x for the velocity u, and z_y for v (the two values are different, in general), we introduce the fluxes per unit length

$$F_x = \int_{z_x}^{z_t} u\,dz, \qquad F_y = \int_{z_y}^{z_t} v\,dz, \tag{28}$$

Given the integral condition (11), it is also valid that $F_x = -\int_{z_b}^{z_x} u\,dz$ and $F_y = -\int_{z_b}^{z_y} v\,dz$, as the circulation is closed in both directions. In dimensionless terms and using the complex notation, we can rewrite the Eq. (28) as

$$\Phi_x = \frac{F_x}{U_0 H} = \int_0^{\zeta_x} \omega_x\,d\zeta, \qquad \Phi_y = \frac{F_y}{U_0 H} = \int_0^{\zeta_y} \omega_y\,d\zeta. \tag{29}$$

Unfortunately, it is not possible to derive a solution for ζ_j (with $j = x, y$) in closed form satisfying the condition $\omega_j = 0$ for the solution (22), (23). However, a numerical algorithm can be easily implemented to perform this computation and obtain the corresponding fluxes. With the same algorithm, we can also compute the crosswise transport predicted by all the classical solutions.

In order to quantify the relevance of Earth's rotation on the development of the secondary circulation, we introduce the ratio

$$r = \frac{\Phi_x}{\Phi_y} \tag{30}$$

between the cross-wind and the longitudinal surface transport. In Fig. 4 the transport in the longitudinal and crosswise directions is shown as a function of ε. As previously seen in the surface velocity plots (Fig. 3), the longitudinal transport Φ_y (Fig. 4a) is not sensitive to rotational effects for $\varepsilon < 1$ and decreases for higher values of ε as the crosswise transport Φ_x grows (Fig. 4b). The classical Ekman approach greatly overestimates the transport along both the x and y direction because it does not take into account the counterbalancing effect of the surface tilt between the lateral boundaries. As for the ratio r computed from (30), Fig. 4c shows that the threshold value of 1 ($\Phi_x = \Phi_y$) is exceeded when the crosswise transport Φ_x reaches its maximum: for increasing values of ε, the crosswise transport induced by rotation is larger than the longitudinal one, and approaches the asymptotic ratio coincident with the classical Ekman solution for $\varepsilon > 10^2$. Both Φ_x and Φ_y tend to zero for large ε, while the ratio r does not. In fact, at an intermediate latitude (with f fixed, i.e. $\sim 10^{-4}$ at 45°), values of $\varepsilon > 10^2$ are achieved either for low turbulent regimes or very deep lakes. In both cases the dimensionless transport goes to zero because transport is scaled by the term $U_0 H = \frac{\tau_0 H^2}{\rho \nu_z}$ (see Eq. (16)), which goes to infinity if $H \to \infty$ or $\nu_z \to 0$. Conversely, the ratio r is not affected by the scaling term, thus providing a good estimation of the relative importance of Earth's rotation. High values of r correspond to cases where the Coriolis force is relevant, while $r = 0$ is obtained for the non-rotating case.

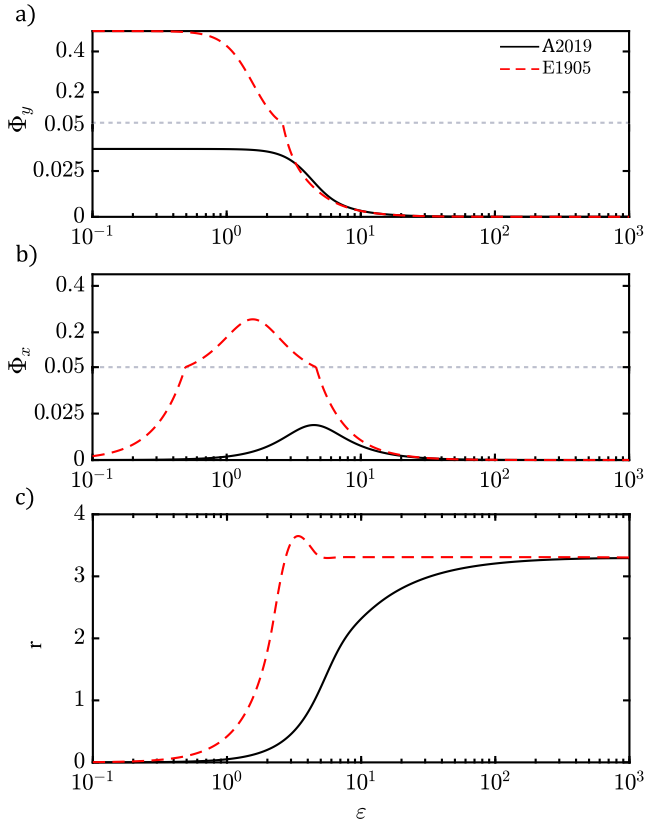

Fig. 4. Dimensionless transport obtained from the analytical solutions A2019 and E1905: (a) longitudinal component Φ_y, (b) crosswise component Φ_x, and (c) ratio r between crosswise and longitudinal transport. Wind aligned with the y axis, no-slip bottom boundary condition. Note: for a better visualization, y axis is plotted with two different scales, separated by the gray dotted line.

Numerical simulations

Analytical solutions provide an exceptional way to understand the fundamental mechanisms governing the phenomena under investigation. However, they are typically based on assumptions that can restrict their application, so their validity has to be demonstrated by comparing them with observations and/or numerical simulations. Here, we used a well-known three-dimensional numerical model to test our one-dimensional analytic solution.

The hydrodynamic model Delft3D-FLOW (Lesser et al., 2004) was used for numerical experiments in the idealized domain. We defined a reference test case and a number of variations which were setup by changing the main parameters of the model (Table 1). For the reference simulation R0, we assumed a domain of width B = 5 km (along x), length L = 50 km along y, and depth H = 50 m (along z), with a total number of 50×500 horizontal cells (resolution of 100 m) and 50 vertical layers of 1 m each. Four groups of simulations were designed, exploring the influence of depth (D1 to D5), width (B1 to B8), vertical turbulence model (v1 to v4 with constant values of ν_z), and horizontal turbulence model (h1 to h7 with constant values of ν_h; h8 with ν_h computed via the default parametrization of Delft3D Horizontal Large Eddy Simulation - HLES). For each case, 14 simulations were run with different values of background latitude, from 0° to 90°N with uneven spacing to effectively capture the variability of the results over the full range of latitudes. From now on, all latitudes will be refereed to the northern emisphere N. Adiabatic (no thermal fluxes considered) simulations were performed with constant water density. The

Table 1
Setup of numerical experiments.

Depth	H [m]	Vert. turb.	ν_z [m^2/s]
D0	50	**v0**	0.0373
D1	10	v1	0.01
D2	30	v2	0.05
D3∗	100	v3	0.1
D4∗	300	v4	0.5
D5 ∗	500		
Width	B [m]	Hor. turb.	ν_h [m^2/s]
B0	5000	**h0**	1
B1∗∗	50	h1	0
B2 ∗∗	100	h2	0.01
B3 ∗∗	200	h3	0.1
B4 ∗∗	500	h4	2
B5	1000	h5	5
B6	2000	h6	10
B7	10000	h7	20
B8	25000	h8	HLES
Reference simulation		**R0 = B0 + D0 + v0 + h0**	
ϕ [°] = 0, 0.05, 0.5, 1, 2, 3, 5, 10, 15, 30, 45, 60, 75, 90			

∗coarser vertical discretization.
∗∗ finer horizontal discretization.

external forcing was prescribed as a constant wind blowing along the main axis of the box, with speed $U_w = 10$ m/s, using a drag coefficient $C_d = 1.7 \times 10^{-3}$ (Wüest and Lorke, 2003).

For the reference simulation R0 the value of the vertical viscosity (v0) was estimated from the numerical results of a k-ϵ free-slip simulation at the intermediate latitude of 45°. The analysis provided the value $\overline{\nu_z} = 3.73 \times 10^{-2}$ m^2/s as a vertical average over the water column. Differently, the reference horizontal eddy viscosity (h0), $\nu_h = 1$ m^2/s, was chosen on the basis of the horizontal resolution of the grid, as suggested by the growth of the oceanic horizontal diffusion with cloud size observed by Okubo (1971). For any additional detail about the implementation of the numerical model we refer to the Electronic Supplementary Material (ESM) Appendix S1.

Results

Analytical solutions vs numerical results

In this section the proposed solution A2019 (22) and (23) is validated against numerical results and compared with three analytical solutions available in the literature: the classic Ekman spiral with finite depth (E1905), the solution provided by Simons (1980) (S1980) assuming the value $\sigma = (3/2)\mathcal{T}$ as in Heaps and Hutter (1984), and the central profile of the two-dimensional solution derived by Toffolon (2013) (T2013).

As a first analysis, we examine how Earth's rotation affects the vertical profiles of the horizontal velocities u and v, considering the reference conditions (R0) and three different latitudes in the numerical simulations (Fig. 5): $\phi = 0°$ (at the equator, $\varepsilon = 0$), $\phi = 45°$ ($\varepsilon = 2.63$), $\phi = 90°$ (north pole, $\varepsilon = 3.13$). The A2019 solution perfectly fits the numerical results for both the crosswise and the longitudinal velocity, and at all latitudes. At the equator (Fig. 5a,b), all solutions for u collapse to zero, as the Coriolis acceleration is absent and wind drives the flow along the longitudinal axis. Moreover, all solutions for v, except for the classic finite depth Ekman solution, have the same vertical structure (25). The omission of the geostrophic term in the classic formulation of the Ekman solution, with the consequent absence of the surface tilt ($\sigma = 0$), determines a linear profile $v/U_0 = 1 - \zeta$. At mid-latitudes, the S1980 solution is still a reasonable approximation for u (Fig. 5c), while it deviates from the numerical result and from

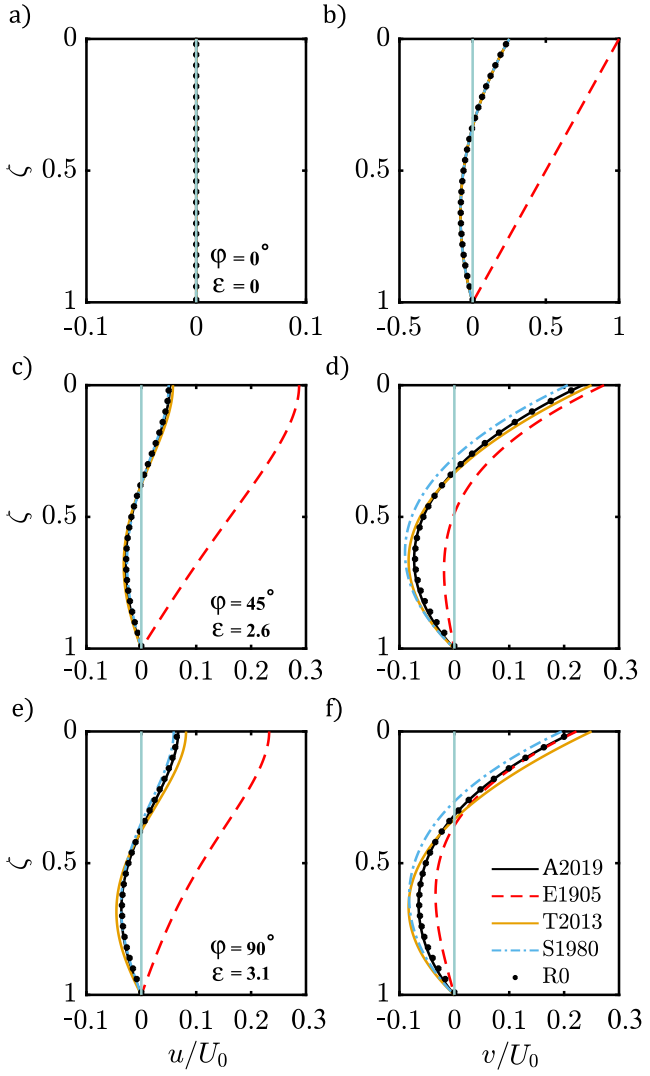

Fig. 5. Vertical profiles of dimensionless velocities u/U_0, v/U_0 obtained from the analytical solutions (A2019, E1905, S1980, T2013) and from the reference numerical simulation R0 at: a, b) $\phi \simeq 0°$ (equator); c, d) $\phi = 45°$; e, f) $\phi = 90°$ (north pole). Wind aligned with the y axis, no-slip bottom boundary condition.

the correct A2019 profile for v, providing smaller velocities. On the contrary, the T2013 solution slightly overestimates the velocities (the reason will be examined in the next paragraph). The mismatch between these solutions (S1980 and T2013) and the numerical results (which coincide with A2019) increases at higher latitudes (Fig. 5e, f).

A more general overview of the different solutions is provided in Fig. 6, where the dimensionless transport Φ_x calculated from numerical simulations is plotted against the parameter ε, and compared with the continuous curves of the analytical solutions. Markers denote numerical outputs whose ID is summarized in Table 1. For each case (same marker), the values of Φ_x are computed for 14 different values of latitude, thus each set includes 14 points.

As a first result, we note that all numerical points lay on the bell-shaped curve provided by the A2019 solution. In the low ε range (< 1, i.e., shallow basins or low latitudes), the A2019 and T2013 solution overlap, while the S1980 and E1905 solutions tend to overestimate the crosswise transport. In fact, both A2019 and T2013 account for the free surface tilt along x, which counterbalances the effect of Coriolis force. Compared to the reference simulation R0, the solution T2013 performs correctly at the lower

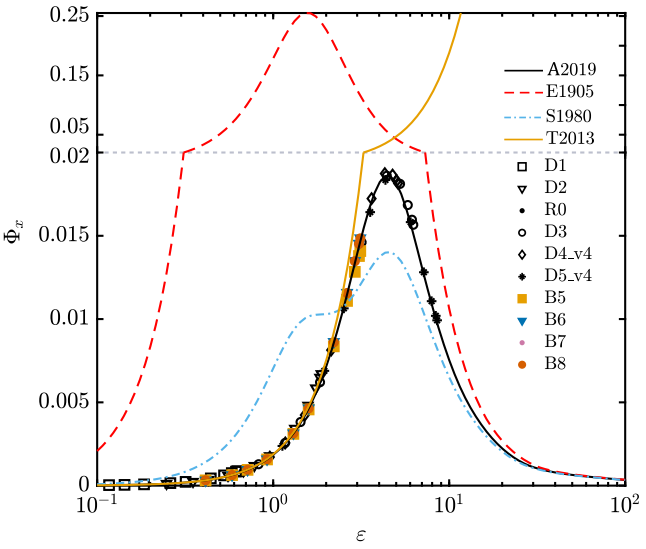

Fig. 6. Crosswise transport Φ_x computed with analytical solutions (A2019, E1905, S1980 and T2013) and from numerical simulations, wind aligned with the y axis, no-slip bottom boundary condition. Note: for a better visualization, y axis is plotted with two different scales, separated by the gray dotted line.

latitudes, where D_E is large and ε is sufficiently small. Beyond its range of validity (say for $\varepsilon > 1$), the T2013 solution diverges from A2019 and overestimates the transport (as already seen for the velocity profiles, Fig. 5c), although behaving reasonably well up to $\varepsilon \sim 2$. In this range of ε, the largest deviation is found for the E1905 and S1980 solutions, with the latter undergoing a transition from an overestimation to an underestimation of Φ_x. For deeper basins, (from D3 to D5, $H \geqslant 100$ m) the T2013 solution is not valid anymore and veers away from the correct bell-shaped behavior by following an increasing monotonic trend. On the contrary, the S1980 approach resembles the correct solution along its downslope, for higher latitudes or depths.

For all existing solutions, the error in the crosswise transport becomes large in the intermediate ε range, where only the A2019 solution behaves correctly, as it does in the whole range of ε.

Effects of the depth

As originally observed by Ekman (1905), the existence of a bottom boundary modifies the shape of the velocity profile and, as a result, the amount of water that is transported orthogonally to the wind forcing. In this section, we analyze the effect of the lake depth on the dimensionless values of velocity and transport.

In Fig. 7a, the dimensionless Ekman spiral is plotted from the simulations performed with different lake depths (colored markered lines) and for the corresponding analytical solution (grey dotted lines), at the reference latitude of 45°. The crosswise velocity u/U_0 is small in shallow basins (D1, D2 and R0 simulations, with H = 10, 30 and 50 m respectively). Its importance relative to the longitudinal component v/U_0 grows with depth until a maximum. The increase of u/U_0 with depth is related to the decreasing effect of bottom friction, which limits the dissipation of the energy coming from the wind to the water column. The maximum extension of the dimensionless Ekman spirals is reached near $H \sim 100$ m (D3 simulation): for larger depths (D4 and D5 simulations, H = 300 and 500 m respectively), the bottom friction becomes negligible and the spiral shrinks because the effect of Earth's rotation does not change the dimensional velocity anymore, while the scale U_0 in Eq. (16) continuously increases with H.

The overall trend is illustrated in Fig. 7b, where the importance of Earth's rotation on the circulation, expressed using the ratio r

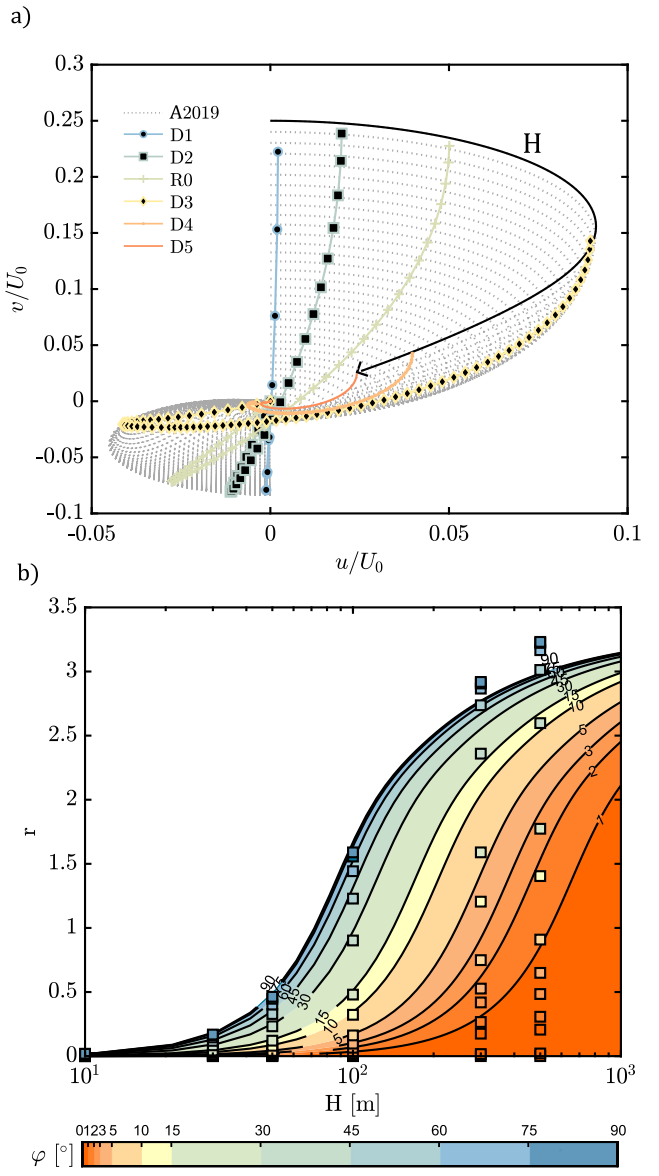

Fig. 7. Effect of the depth reconstructed from numerical simulations and the analytical A2019 solution: a) dimensionless Ekman spirals for all simulations with varying depths at the reference latitude $\phi = 45$°N (colored marked lines) and analytical solution (dotted grey lines); b) ratio r of dimensionless transport plotted as a function of latitude and depth from numerical simulations (colored squares) and from the analytical solution (contour plot). (For interpretation of the references to colour in this figure legend, the reader is referred to the web version of this article.)

from Eq. (30), is shown as a function of depth at different latitudes for simulations (squares) and the analytical solution A2019 (contour plot). The ratio r grows with both depth and latitude in a continuous way, asymptotically approaching to the infinite depth case (see Fig. 3 and 4). The A2019 solution provides a good estimation of the crosswise transport, but the perfect matching between the analytical solution and the numerical results is lost for the two deepest cases (D4, D5), where some of the assumptions of the analytical solution are not satisfied as will be discussed in Section "Limits of the analysis". However, these results show that for a given value of eddy viscosity, latitude and depth play together a fundamental role: lakes located at low latitudes have to be very deep to experience the maximum effect of Earth's rotation, which conversely is more easily achieved in shallower lakes at mid and high latitudes.

Effects of the width

The analytical solution A2019 suggests that the width of the basin does not affect the velocity profile. In fact, the A2019 solution relies on the assumption that the crosswise transfer of momentum is unimportant, a condition that is not valid for narrow lakes where the horizontal viscosity is high, as extensively discussed by Toffolon (2013) in the case of small ε. In this section, we examine how the width affects the circulation pattern due to the presence of lateral boundary layers.

Analogous to the previous analysis on the role of the depth (Fig. 7a), Fig. 8a shows the behaviour of the dimensionless spiral as the width changes, considering the reference latitude (45°) and different widths, from 50 m (B1) to 25 km (B8) and including R0 (5 km). For the range of widths $B > 1$ km (B6, B7, B8 and R0), the crosswise transport is independent of the horizontal extent of the basin, and only increases with latitude. This trend is clear from Fig. 8b, where the ratio r is plotted as a function of width at different latitudes. The A2019 solution well captures the magnitude of crosswise transport for these relatively wide cases.

However, simulations with a narrower domain (width < 1 km, B1 to B5) show weaker crosswise transport (Fig. 8a). This is illustrated in Fig. 8b which shows a mismatch between the numerical and analytical solutions, in the first case the ratio r being smaller than in the latter. In the numerical solution, the crosswise transport decreases for narrower lakes, as a result of the increased internal friction due to the horizontal velocity gradients. In the next section, the reasons behind this mismatch are addressed by taking into account the role of the lateral boundary layers.

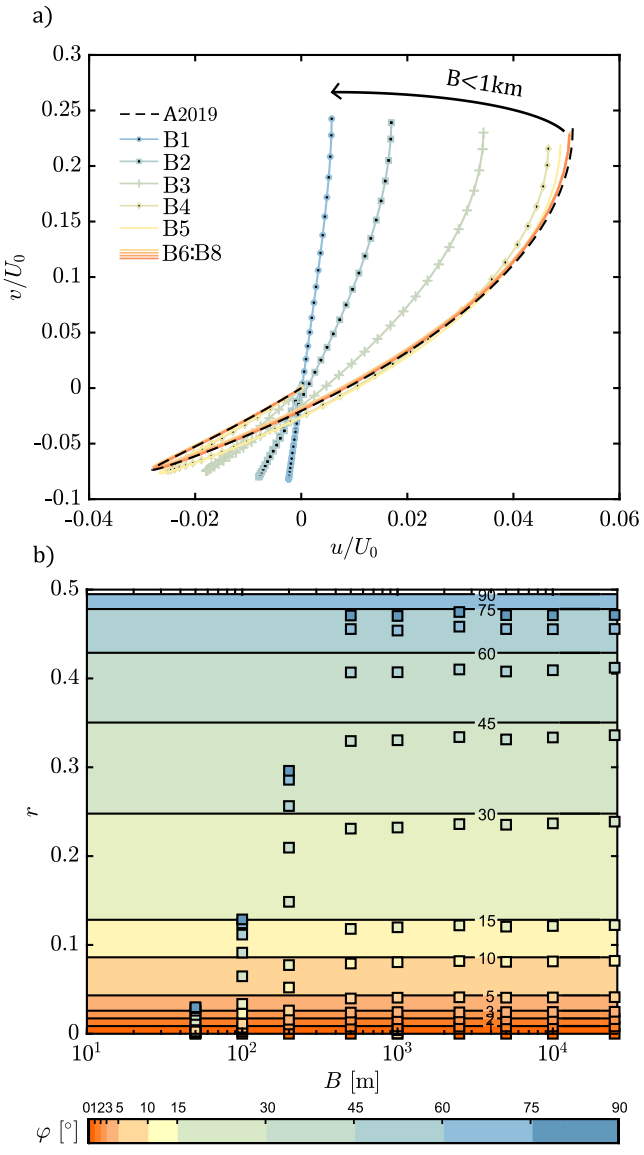

Fig. 8. Effect of the width reconstructed from numerical simulations and the analytical A2019 solution: a) dimensionless Ekman spirals for all simulations with varying widths at the reference latitude $\phi = 45°$N (colored marked lines) and analytical solution (dashed black line); b) ratio r of dimensionless transport plotted as a function of latitude and width from numerical simulations (colored squares) and from the analytical solution (colored lines). (For interpretation of the references to colour in this figure legend, the reader is referred to the web version of this article.)

Effect of eddy viscosity and boundary layers

As we have seen before, the results obtained from the numerical model and from the analytical solution A2019 clearly diverge for the case of narrow lakes. Building on previous studies (Toffolon, 2013), we can associate this discrepancy to the combined effect of the cross-section's aspect ratio and of turbulence anisotropy on the development of the secondary circulation. This issue is tightly connected with the estimate of the eddy viscosity (a parameter of difficult estimation, especially along the horizontal dimension, see e.g. Toffolon and Rizzi, 2009). Here we examine the direct effect of the value of the eddy viscosity (both vertical and horizontal) on velocity and transport.

The traditional approach for estimating the vertical eddy viscosity (ν_z) is through the evaluation of the depth of the wind-induced motion (Madsen, 1977; Csanady, 1982; Heaps and Hutter, 1984), which is commonly represented by the Ekman depth when rotational effects are taken into account. Therefore ν_z, in unstratified conditions, can vary according to the latitude, depth and wind stress. A reference value can be determined as a function of the Coriolis parameter f and the surface friction velocity $u_* = \sqrt{T_0/\rho}$ as

$$\nu_z = K\frac{u_*^2}{f}, \tag{31}$$

where the dimensionless coefficient K is 0.008 in Heaps and Hutter (1984), 0.005 in Csanady (1976) and 0.026 in Svensson (1979). According to Eq. (31), ν_z increases as latitude decreases, leading to $\nu_z \sim 5 \cdot 10^{-1}$ m^2/s at $\phi \simeq 45°$ (assuming $u_* \sim 10^{-2}$ m/s), a large value that is not commonly encountered in real lakes. Hence, we performed a sensitivity analysis to understand the influence of this parameter.

The effect of changing ν_z on the vertical profile of the crosswise velocity is illustrated in Fig. 9a for the deep D4 domain at the reference latitude $\phi = 45°$, considering both numerical simulations and the A2019 solution. By increasing ν_z (cases ν3 and ν4, 0.1 and 0.5 m^2/s respectively) the dimensionless crosswise velocity increases together with the thickness of the surface layer set in motion by the wind. Conversely, for lower ν_z (cases ν0 to ν2, order of magnitude 10^{-2} m^2/s) the circulation is limited to the top layer and the u/U_0 is smaller because the scale U_0 increases with decreasing ν_z. The A2019 solution captures well the shape of the velocity profile, hence the amount of water transported.

Then, we examined the effect of changing the value of the horizontal eddy viscosity. We recall that all simulations presented so far were performed with the same value of $\nu_h = 1$ m^2/s. In Fig. 9b, the profiles of crosswise velocity u/U_0 are plotted for simulations h1 to h8, where the value of the horizontal eddy viscosity was changed for the narrow domain B4 (i.e., B = 500 m). The crosswise velocity decreases when increasing ν_h, as mixing is enhanced at the expense of horizontal gradients. Therefore, the momentum

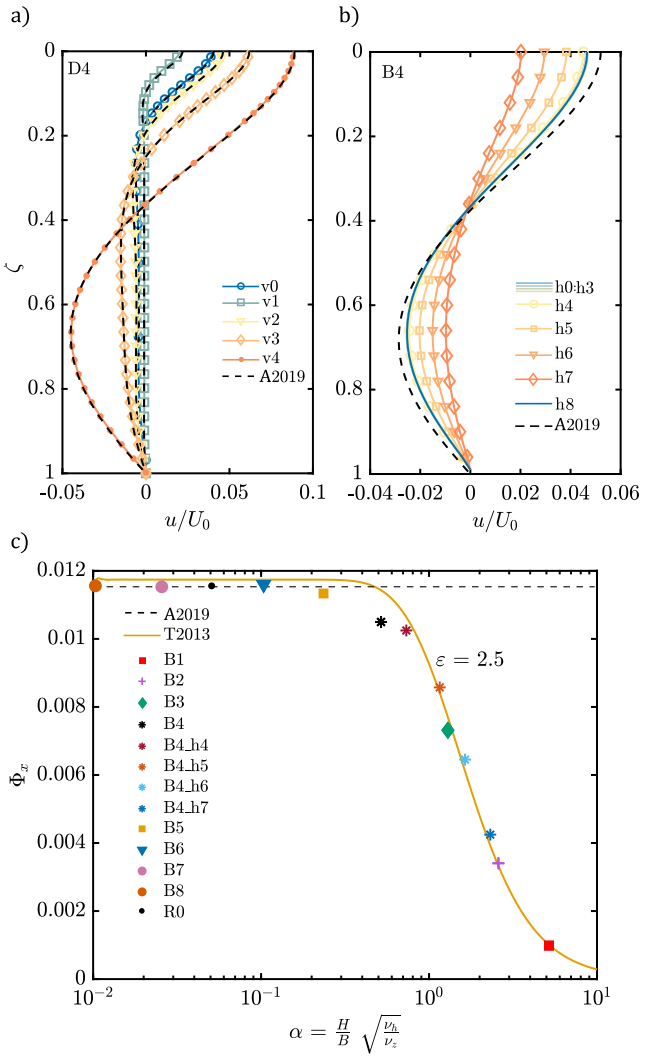

Fig. 9. Effect of turbulence parameters at the reference latitude $\phi = 45°$N. Top plots: dimensionless crosswise velocity u/U_0 from numerical simulations (colored marked lines) and A2019 analytical solution (black dashed lines), a) deep D4 simulations (H = 300 m) with varying vertical eddy viscosity (v0 to v4), and b) narrow B4 simulations (B = 500 m) with varying horizontal eddy viscosity (h0 to h8). Bottom plot c): dimensionless transport Φ_x against the anisotropy parameter α (Toffolon, 2013), for all B- and h-type simulations (scatter plot), and the A2019 (black dashed line) and T2013 (continuous orange line) analytical solutions for the corresponding ε value. (For interpretation of the references to colour in this figure legend, the reader is referred to the web version of this article.)

transfer from the lateral boundaries to the center of the lake is more effective and velocity is reduced along the water column due to the decelerating effect of the down-welling and up-welling regions. For small values of ν_h the lateral boundary layers are very thin and the central profile of u/U_0 approaches the one predicted by the A2019 solution.

In order to have a guideline in the interpretation of the results, we refer to the complete solution proposed by Toffolon (2013), which accounts for the role of ν_h by means of a combined geometry-anisotropy parameter (Toffolon and Rizzi, 2009),

$$\alpha = \frac{H}{B}\sqrt{\frac{\nu_h}{\nu_z}}. \tag{32}$$

Such a parameter represents the ratio of the vertical (H^2/ν_z) and the horizontal (B^2/ν_h) temporal scales of the diffusion of momentum, and subsumes the effect of the boundary layers at the surface/bottom and at the lateral walls of the domain.

Fig. 9c analyzes the variation of the crosswise transport Φ_x versus α, by changing B and ν_h at the reference latitude 45°. The plateau at the left-hand-side part of the graph ($\alpha \leqslant 10^{-1}$) applies to scenarios B6 to B8, including the reference simulation R0, where the width is larger than 1 km and the numerical transport follows the behavior of the A2019 solution. In this range of widths and for the reference values of ν_h and ν_z, the transport is independent of width and of the effect of the horizontal/vertical boundaries. Differently, the transport decreases exponentially for smaller widths or larger ν_h as the parameter α increases, in good accordance with the complete analytical solution proposed by Toffolon (2013).

Discussion

The governing scales

The aim of this work was to analyze the parameters that primarily affect the secondary flow resulting from the interaction of wind forcing and the Coriolis force. As seen in the previous sections, the proposed A2019 solution correctly reproduces the numerical results in most cases, with the exception of narrow lakes with large horizontal viscosity where boundary layer effects become important. Neglecting these particular cases, the general validity of the A2019 solution suggests that for a wide range of depths and widths it is possible to predict how much water is likely to be moved by the Coriolis force, and whether Earth's rotation will affect the flow field or not, as a function of the Ekman number $\mathrm{Ek} = H/D_E$, or the equivalent parameter ε, solely.

In Fig. 10a, the ratio r is plotted as a function of the actual depth H and the Ekman depth D_E, showing in which range of these two variables the Coriolis acceleration is expected to be important. For a lake at a given latitude and specified turbulent regime, the Ekman depth can be easily computed. Then, the magnitude of the crosswise transport (and consequently of the up-/down-welling) can be determined based on the depth of the lake. The range where the crosswise transport due to Earth's rotation is relevant grows with the depth of the basin and with the Ekman depth. We note that the value assumed for the vertical eddy viscosity is particularly important, as D_E is proportional to $\nu_z^{1/2}$.

When analyzing the effect of the horizontal extent of the basin on the flow regime, the importance of the horizontal eddy viscosity was stressed. In fact, the crosswise transport in narrow lakes decreases due the horizontal friction and the presence of lateral boundaries in the same way as it is limited by the bottom friction in shallow lakes. In this process the lake width affects the horizontal momentum transfer, and should be taken as an important length scale. However, as we demonstrate in Fig. 9c, the reason to consider the role of the width B in this phenomenon is not the one usually perceived as important.

Indeed, a criterion often proposed to discriminate if the Earth's rotation will affect the flow field (hence, the transport) is when the lake width is larger than the Rossby radius $R = U/f$, that is when the Rossby number Ro is lower than unity. Here we show that this is not correct for the wind-driven steady circulation in lakes. In Fig. 10b the ratio r from all simulations is plotted as a function of the Rossby radius R and the width B. We note that at B = 50 m and B = 5000 m markers have been spaced out for a better visualization. In the case of fixed H and different B (squares, Bx simulations) the increase of crosswise transport with R is only driven by the variation in latitude, as the horizontal extent of the lake does not affect the relative importance of Earth's rotation on the secondary circulation. Hence, for a given Rossby number, different values of crosswise transport can be found: as an example, the black line where $R = B$ intersects squares of different colors. As discussed in Section "Effect of eddy viscosity and boundary layers", in the range of narrow lakes

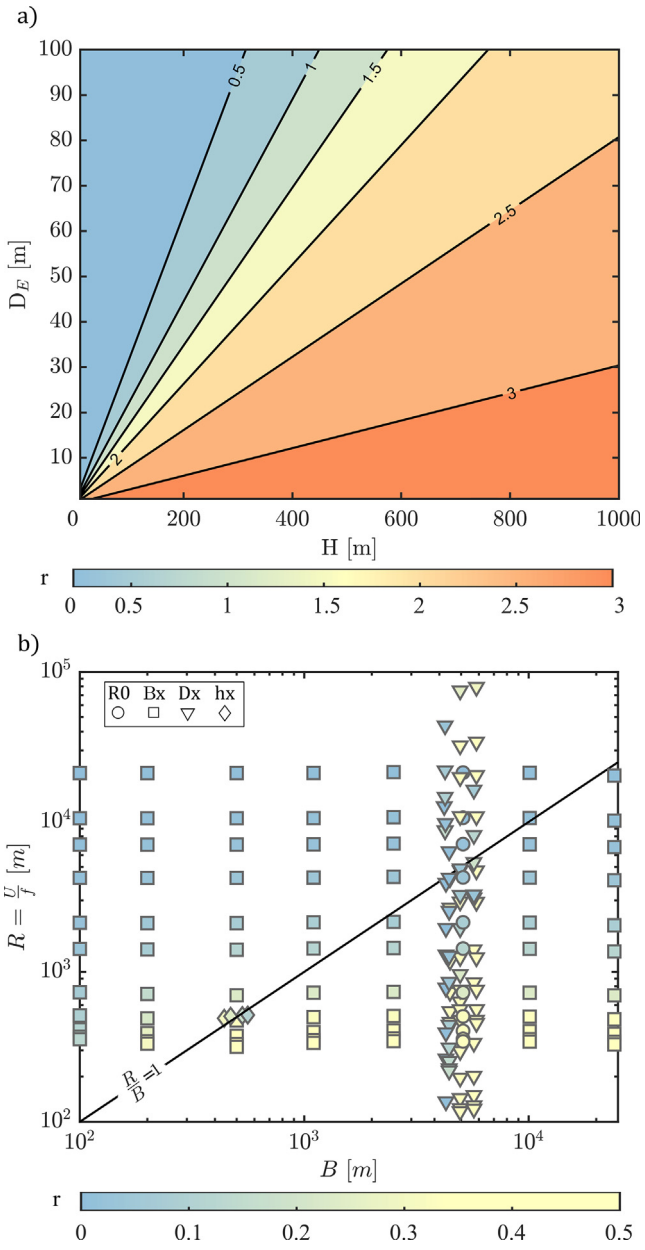

Fig. 10. Ratio r of the crosswise transport along the two horizontal directions plotted as a function of a) the Ekman depth D_E and depth H; b) the Rossby radius R and width B. Note: in b) diamonds, circles and triangles have been spaced out for a better visualization: R0, Dx and vx sets are associated to B = 5000 m and hx to B = 500 m.

the crosswise transport is smaller due to the effect of the boundary layers and anisotropy, and this effect is not taken into account in the computation of Rossby radius. In fact, if ν_h changes (diamonds), the relevance of Earth's rotation r can vary even if Ro is the same. If B is fixed and H changes (triangles), the magnitude of the Coriolis-induced transport can be high (yellow colored markers) or low (blue markers) both for Ro < 1 and Ro > 1. Then, the computation of the Rossby number cannot give any insight on how much Earth's rotation affects the Ekman transport in a closed basin.

Limits of the analysis

In this paper, a one-dimensional steady solution was derived for quantifying the crosswise transport occurring in an elongated basin due to Earth's rotation, in unstratified and horizontally homogeneous conditions. The domain was assumed as rectangular with a flat bottom, both choices being an important simplification of a realistic lake, especially when compared to other idealized models available in literature, which consider linear, triangular and even more complex bathymetries (e.g. Simons, 1980; Winant, 2004; Sanay and Valle-Levinson, 2005). However, on the one hand the simplification of a flat bottom significantly reduces the number of degrees of freedom of the analysis and let us focus purely on the large-scale wind-driven circulation. On the other hand, a rectangular domain is a rather common idealization for elongated enclosed or semi-enclosed basins (e.g. Kasai et al., 2000; Ponte, 2010). The crucial aspect in our analysis is that the existence of lateral boundaries controls the development of a crosswise transport, overcoming the limits of the traditional Ekman transport solutions derived for 'infinitely large lakes or oceans' (Hutter et al., 2011). We refer the reader to more detailed approaches for the accurate representation of topographic effects when irregularities in the horizontal shape of the basin may affect the development of the circulation (e.g. Mohammed-Zaki, 1980).

While presenting the results, we encountered a few cases where the one-dimensional approach embedded in the A2019 solution leads to inaccuracies in the estimation of the crosswise transport, in particular for very deep cases ($H > 300$ m). We observed that these inaccuracies are related to the key assumption that the circulation is closed (i.e., null integral) in the central water column of the lake, which is not satisfied. Such an assumption is a simplified version of the general constraint that a steady flow in a closed domain must have a null exchange across any surface dividing the domain in two parts, and is valid only when the flow field is characterized by some symmetry in the cross-section. For more detailed analyses, two-dimensional (e.g. Dever, 1997; Toffolon, 2013) and three-dimensional solutions (e.g. Winant, 2004; Ponte, 2010) are available for a precise reconstruction of the flow field, but this is not the main scope of this work.

Considering a steady state is the fundamental assumption, because the stationarity is the prerequisite for the integral condition to be valid and thus for the inclusion of the lateral boundaries. We are not interested in the temporal development of the flow field, which can be studied with time-varying solutions specifically designed for that purpose (e.g. Fjeldstad, 1930; Hidaka, 1933; Platzman, 1963; Madsen, 1977). The numerical results show that in many cases an equilibrium condition is achieved after a spin-up time that varies from some hours to some days of constant and uniform wind, a condition that many lakes experience from local breezes to large-scale synoptic winds.

We are aware that the assumption of constant eddy viscosity (together with that of constant density) is quite limiting. Some efforts were spent to overcome the gaps related to the definition of ν_h and ν_z in analytical formulations (e.g. Thomas, 1975; Madsen, 1977; Svensson, 1979), but definitive results are not suitable for the derivation of a simple analytical solution in closed form.

Finally, the one-dimensional solution we derived provides an analytical quantification of transport orthogonal to the main flow when wind blows along the main axis of elongated lakes. The numerical results suggest that, despite the simplifications we adopted, such a solution is suitable for simplified three-dimensional domains in unstratified conditions, which typically occurs in many real lakes although with different frequency depending on their mixing regime. Also, long-lasting wind events aligned with the main axis of a lake are common for elongated lakes (e.g. Lake Baikal, Lake Erie, Lake Ontario, Lake Constance, northern Lake Garda), where steady currents of the kind discussed here have been already modeled and observed (Rao and Murty, 1970; Gedney and Lick, 1972; Wang et al., 2001; Amadori et al.,

2018; Piccolroaz et al., 2019) and in some cases shown to significantly contribute to deep mixing (Boehrer and Schultze, 2008; Schmid et al., 2008; Tsimitri et al., 2015; Piccolroaz and Toffolon, 2018; Piccolroaz et al., 2019). Hence, such a simple, even though limited, analytical tool could help in estimating to what extent crosswise up/down-welling ascribed to Earth's rotation can be relevant for the transport and mixing processes of a lake.

Conclusions

In this contribution an analytical solution was derived to help identifying the scales that determine the importance of Coriolis acceleration as a driver of transport in non-stratified lakes. We showed that the Ekman number (i.e. the ratio of the actual depth of the lake and the Ekman depth) controls whether Earth's rotation will affect the steady circulation in a lake of given size at in a given geographical location and therefore should be used as a governing scale instead of the Rossby number. Consistently with some previous findings (Kasai et al., 2000; Sanay and Valle-Levinson, 2005; Valle-Levinson, 2008), we identified the parameter ε, which is directly proportional to the Ekman number, with the novelty of including in the analysis the size of the lake, the turbulent mixing and the effect of a closed domain. The combined analytical and numerical analysis we carried out in this contribution allows for the following final conclusions:

1. Coriolis force is important also in narrow lakes and produces a crosswise Ekman transport that can be analytically quantified if the effect of lateral boundaries is taken into account through a null flux condition.
2. The steady crosswise transport is scaled by the Ekman number, which is defined once the depth of the lake, the vertical eddy viscosity and the latitude are defined. Such a crosswise transport is responsible for up- and down-welling phenomena at the lake sides.
3. The Rossby number *Ro* does not provide any useful information about the development of Ekman currents in enclosed basins. The use of a horizontal length scale is appropriate only when the lateral boundary layer is large enough to affect the secondary circulation: in that case, a frictional length scale is needed, bringing into play the horizontal eddy viscosity and requiring the use of an anisotropy parameter like α proposed by Toffolon (2013).

Declaration of Competing Interest

The authors declare that they have no known competing financial interests or personal relationships that could have appeared to influence the work reported in this paper.

Acknowledgement

Part of the simulations were carried out on the Cartesius supercomputer at SURFsara (www.surfsara.nl).

Literature review on Ekman transport

A brief review of the state of the art about the effect of Earth's rotation on steady circulation in lakes can be useful to frame the analytical problem and to get rid of any prejudice on its application to enclosed real basins. The original work of Ekman (1905) was derived for infinitely deep and wide rotating systems (as the ocean can be approximated) subject to constant and uniform wind. To the other extreme, analytical solutions were proposed for idealized narrow rectangular lakes (e.g. Heaps and Ramsbottom, 1966) or enclosed basins with variable bathymetry (e.g. Csanady, 1982), but neglecting the effect of rotation. The path from Ekman's original solution to the description of steady currents in real enclosed basins was certainly long, but for the range of intermediate conditions several generalizations of the original Ekman theory have been proposed (see also Simons, 1980; Hutter et al., 2011; Defant, 1962 for a review). Finite-depth and time-dependent solutions followed the initial suggestion available in Ekman's work (Fjeldstad, 1930; Hidaka, 1933; Platzman, 1963; Madsen, 1977), together with the inclusion of horizontal pressure gradients associated to wind set-up (Welander, 1957; Birchfield, 1972), which were particularly relevant for the case of enclosed basins and were successfully applied to describe circulation in large lakes (Gedney and Lick, 1972). Additional complexity was added by taking into account density stratification (Lee and Ligget, 1970), with relevant contributions from estuarine studies (Kasai et al., 2000; Valle-Levinson et al., 2003), and non constant vertical turbulence (Thomas, 1975; Madsen, 1977; Svensson, 1979). A few analytical studies specifically focused on narrow, elongated and deep basins (such as glacial and rift valley lakes) with homogeneous water, which is a condition that dimictic lakes experience twice a year. For these lakes, some analytical works predict the development of intense closed circulation, orthogonal to the wind direction and forced by the presence of lateral boundaries, with consequent significant coastal up- and down-welling (Simons, 1980; Winant, 2004; Ponte, 2010; Toffolon, 2013).

Analytical, numerical and observational studies followed to define the role of Earth's rotation on horizontal and vertical circulation in closed basins, with diverse and sometimes contradictory results which enhanced the confusion on the relevant length scales. In estuarine applications, the lateral distribution of the flow in semi-enclosed basins was well investigated by a wide number of studies. To the purposes of the present work, a milestone is represented by the analytical study of Kasai et al. (2000), who questioned the conventional assumption of the Rossby radius as a predictive parameter for the development of rotational currents. They demonstrated that Earth's rotation can be less important than density gradients also in basins where the width is larger than Rossby radius. In order to quantify the effects of Coriolis acceleration in steady circulation, they used the Ekman number Ek. The main conclusion of their work was that when Ek is small (i.e., $H < D_E$), the whole water column is inside the Ekman layer and the flow is governed by viscosity effects. When Ek is large ($H > D_E$), a part of the water column is not in geostrophic balance and is affected by Coriolis force. Following this result, the numerical work by Sanay and Valle-Levinson (2005) confirmed that in homogeneous, rotating basins the Ekman depth is a predictive scale for the development of transverse circulation, as those predicted by Winant (2004). This achievement was then extended to the stratified case by Valle-Levinson (2008), where the relative importance of the basin's width and depth was discussed for density-driven exchanges. Some years later, Ponte et al. (2012) observed a similar transverse circulation in the Gulf of California. In the same context, Cheng and Valle-Levinson (2009) compared the magnitude of lateral advection and Coriolis acceleration by means of numerical experiments in basins of different sizes. By quantifying the terms of the momentum equation as functions of Ekman and Rossby numbers, they observed that lateral advection is relevant in narrow and deep basins (large Ro and Ek) and decreases with mixing (large ν_z), while the relevance of the Coriolis term increases in wider basins (small Ro) and is less sensitive to the depth.

Earth's rotation was also taken into account for investigating gravity currents caused by riverine intrusions (we refer to

Griffiths (1986) for an extensive review). In particular, interesting studies on relatively narrow lakes in unstratified (Pilotti et al., 2018) and stratified (Laborde et al., 2010) conditions revealed the existence of relevant deflections of the river plume to the right-hand shoreline (in northern hemisphere). The scaling suggested by the authors was based on Rossby radius, computed as U/f where U was taken as the inflow velocity. Despite the limited width of the basins, the Rossby number in the cited works was found to be much smaller than 1, as the inflow velocity was extremely low (generally $\sim$1 cm/s), hence Coriolis acceleration acts on the flow path of riverine intrusions in the same way as for inertial currents.

The relative importance of the internal wave field vs geostrophic currents (i.e., density stratification vs steady state currents) was investigated in oceans (Veronis, 1956) and enclosed basins (Stocker and Imberger, 2003) through analytical approaches based on energy partitioning (Antenucci and Imberger, 2001) as a function of the Burger number $S = NH/(fL)$, with N the buoyancy frequency. By splitting the total energy budget into a geostrophic component and a set of cyclonic and anticyclonic waves, these studies found that low Burger numbers and long lasting winds were the condition for the geostrophic component to dominate on density driven waves, but the effect of Earth's rotation on the steady geostrophic current was not taken into account.

Besides the studies based on the basin's size, some analyses focused on the role of time scales for the rotational response of the basin. Amongst these, Mohammed-Zaki (1980) solved analytically the momentum and continuity equations under the assumptions derived from Ekman theory in the case of deep basins ($Ek \gg 1$) and observed that the steady state solution is achieved under uniform wind forcing after a diffusive time scale proportional to the Ekman number and independent on the lake's horizontal extent. An inverse frictional timescale, scaled again with the Ekman number, was then introduced by Dever (1997), controlling the vertical structure of the wind-driven response to the Earth's rotation in the cross-shelf circulation of the Northern California Shelf. Differently, Ponte (2010) linked the rotational response of the basin to the frequency of the wind forcing in such a way that the Ekman transport is triggered only in the 'sub-inertial range', when the frequency of the wind forcing is smaller than inertial frequency.

Interestingly, also the contributions described above were made under the assumption that the horizontal dimension of the basin is smaller than the barotropic Rossby radius of deformation. However, we should recall that "it is not just the horizontal extent of a basin, but its depth which dictates whether the Earth's rotation affects the circulation of a water body" (Hutter et al., 2011). Hence, shall we include the Coriolis acceleration when investigating steady circulation in relatively small lakes? And what does "small" mean? Citing Hutter et al. (2011) again, few kilometers horizontal extent seem to be enough for rotational effects to be relevant in a basin of at least 50 m depth. Nevertheless, since a horizontal scale other than the Rossby radius (whatever defined) is still missing, the issue on the meaningful scales for wind-driven steady currents in enclosed basins on a rotation Earth is still open and deserves a conclusive answer we tried to give in this contribution.

Analytical solution for free-slip boundary condition

In this section the A2019 solution is derived for the case of free-slip bottom boundary condition. For consistency with the main text, the free-slip version of the equations provided here are numbered as the corresponding no-slip equations in the main text, after the letter 'B'.

In the case of free-slip boundary condition, zero tangential stresses are applied to the bottom ($z = z_b$) and Eq. (B.10) are combined to the differential problem composed by (7) and (8), with (9) as surface boundary condition.

$$\left.\frac{\partial u}{\partial z}\right|_{z=z_b} = 0, \qquad \left.\frac{\partial v}{\partial z}\right|_{z=z_b} = 0. \tag{B.10}$$

The complex formulation of the problem (12) is then complemented with the bottom boundary condition (B.13), the surface boundary condition ($z = z_t$) in (13) and the integral condition (14).

$$\left.\frac{\partial W}{\partial z}\right|_{z=z_b} = 0. \tag{B.13}$$

By applying the scales (16) and according to the dimenionless problem (15), we formulate the corresponding dimensionless free-slip boundary condition

$$\left.\frac{\partial \omega}{\partial \zeta}\right|_{\zeta=1} = 0. \tag{B.19}$$

The differential problem we need to solve is therefore composed by the differential Eq. (18) and by the surface (19), bottom (B.19) and integral (20) boundary conditions. The general solution to the dimensionless problem can be written as a function of σ and ε as follows:

$$\omega(\zeta) = \frac{\cos\left[\Theta(\zeta-1)\right]}{\Theta \sin\Theta}\mathcal{T} + \frac{\sigma}{\Theta^2}. \tag{B.22}$$

By forcing the solution (B.22) to satisfy the integral condition (20) we obtain the free-slip case σ:

$$\sigma = \mathcal{T}, \tag{B.23}$$

which results to be independent on ε and therefore on Earth's rotation. Here the surface slope is indeed counterbalanced by the tangential wind stress only, as zero tangential stresses are considered at the bottom. Thus, the solution for the surface slope obtained by applying the integral condition (20) and free-slip bottom boundary condition (B.19) is the same as in Heaps and Hutter (1984), which is computed by assuming a closed integral in the direction of wind only (in our case $\int_0^1 \frac{v}{U_0} d\zeta = 0$).

In the limit case of low ε, we consider the case of very shallow lakes, where the shallowness is defined with respect to the Ekman depth ($H \ll D_E$). By substituting the expression of σ (B.23) in Eq. (B.22), the solution for very small values of ε and therefore of Θ is given by Eq. (B.25):

$$\frac{\omega}{\Upsilon} = -\frac{1}{2}\zeta^2 - \zeta + \frac{1}{3}. \tag{B.25}$$

which is the usual velocity profile induced by wind stress in a non-rotating system (e.g., Heaps and Hutter, 1984).

Flow field and crosswise transport

For consistency with the main text, the solution is discussed assuming a wind aligned with the y axis of the domain, such that $\mathcal{T} = i$. The behaviour of surface velocity obtained from Eq. (B.22) by imposing $\zeta = 0$ is plotted in Fig. B1 and compared with the Ekman solution in the finite depth version. The along-wind motion ω_y coincides for both solutions, being larger for low values of ε and decreasing for increasing ε. The crosswise flow ω_x follows divergent paths: the E1908 solution goes to infinity for small values of ε, while the A2019 solution follows a bell-like curve similar to the no-slip case (see Fig. 3 in the main text), but with a lower minimum. In the range of ε where ω_x increases, ω_y decreases until the same magnitude is reached and the surface water moves at 45° to the right of the wind as in the Ekman spiral theory. As previously

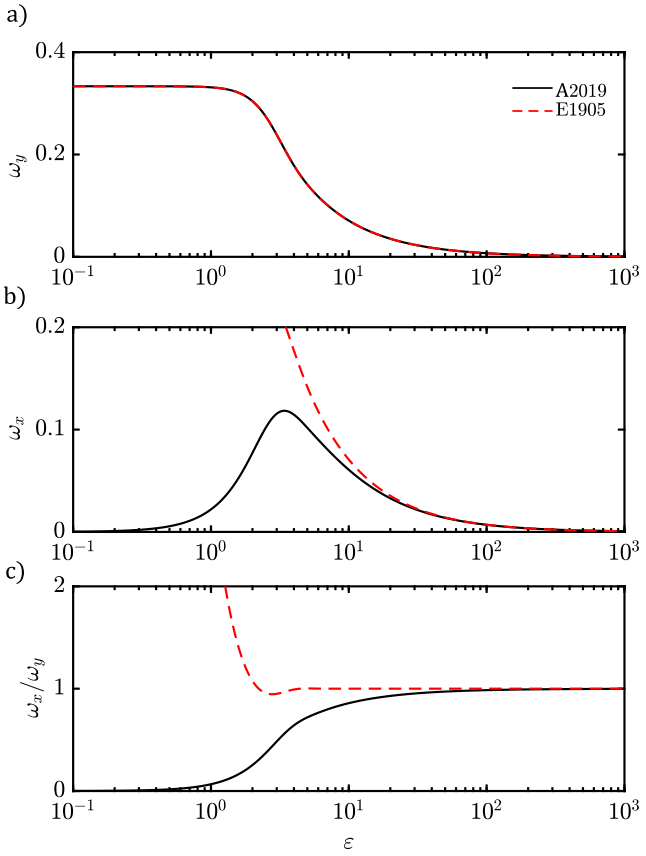

Fig. B1. Dimensionless surface velocity obtained from the analytical solutions A2019 and E1905: (a) longitudinal component ω_y, (b) crosswise component ω_x, and (c) direction. Wind aligned with the y axis, free-slip bottom boundary condition.

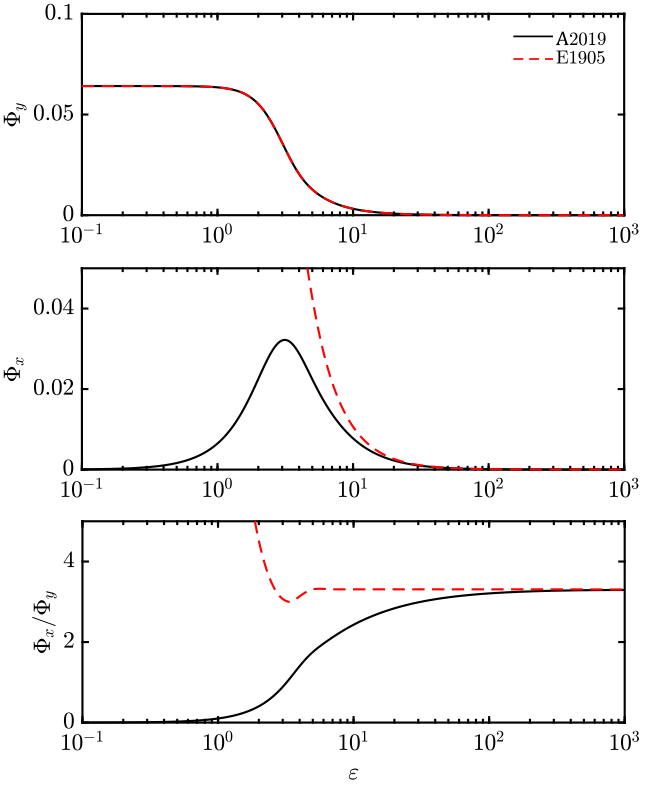

Fig. B2. Dimensionless transport obtained from the analytical solutions A2019 and E1905: (a) longitudinal component Φ_y, (b) crosswise component Φ_x, and (c) ratio r between lateral and longitudinal transport. Wind aligned with the y axis, free-slip bottom boundary condition.

seen in the no-slip case, the classical Ekman approach correctly describes the motion for large values of ε (deep lakes, high latitudes and/or weak mixing regimes), but it overestimates the velocity in both directions within the range of lower ε.

If transport is numerically computed as in Eq. (29), the behaviour of longitudinal and crosswise transport from the supported solution can be studied also in the free-slip case. In Fig. B2 Φ_y in the along-wind and Φ_x in the crosswise direction is shown as a function of ε. As for surface velocities plots (Fig. B1), the along-wind transport Φ_y is not sensitive to rotational effects for $\varepsilon < 1$ and decreases for higher values of ε as the crosswise transport Φ_x grows. If the ratio Φ_x/Φ_y is computed, the threshold value of 1 is exceeded when the crosswise transport Φ_x reaches its maximum: for increasing values of ε, the crosswise transport induced by rotation is larger than the longitudinal one and approaches the asymptotic ratio, which coincides with the traditional Ekman solution.

Validation against numerical results

For a comparison between the analytical solution and the numerical simulations the reference simulation R0 (see Table 1

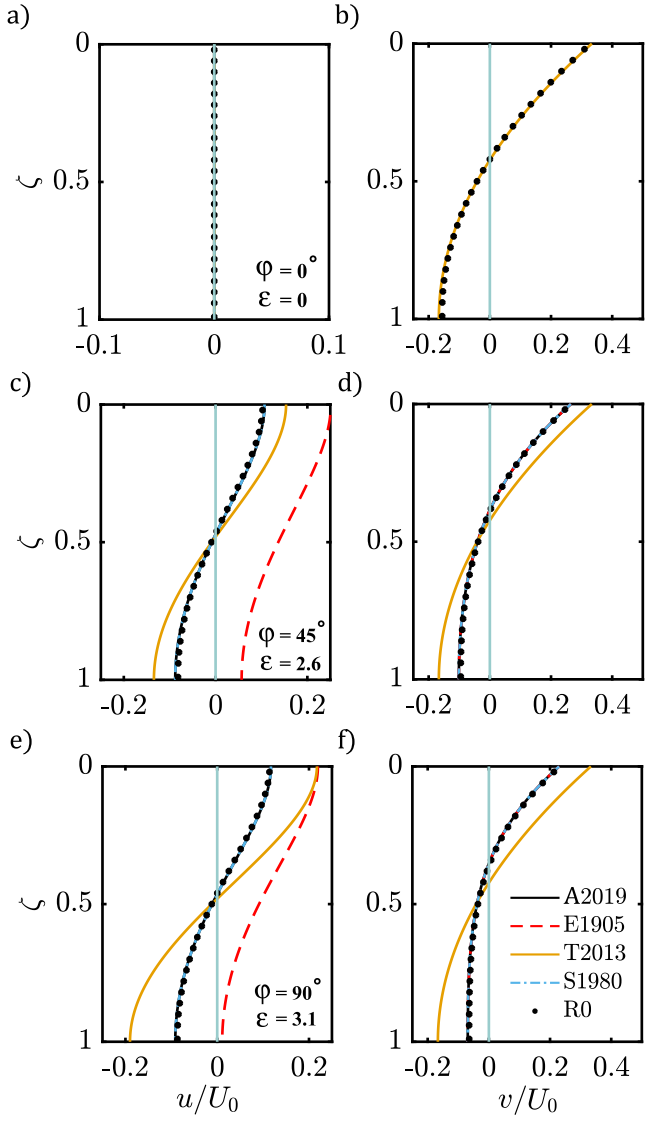

Fig. B3. Vertical profiles of dimensionless velocities u/U_0, v/U_0 obtained from the analytical solutions (A2019, E1905, S1980, T2013) and from reference numerical simulation R0 at a, b) $\phi \simeq 0°$ (equator), c, d) $\phi = 45°$, e, f) $\phi = 90°$ (north pole). Wind aligned with the y axis, free-slip bottom boundary condition.

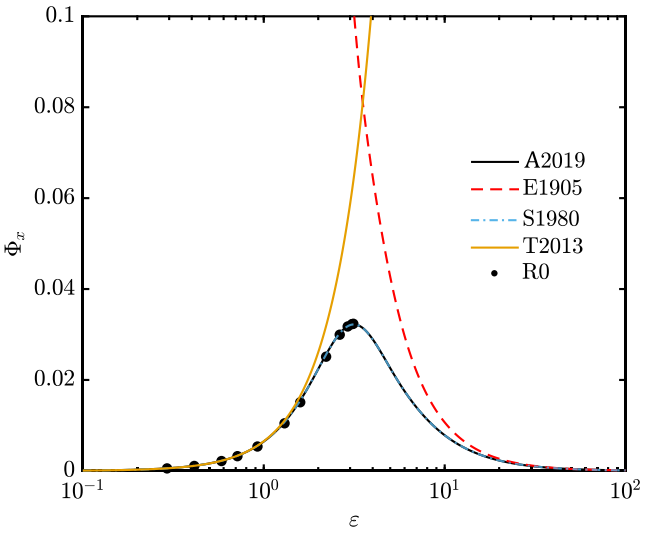

Fig. B4. Crosswise transport Φ_x computed with analytical solutions (A2019, E1905, S1980 and T2013) and from numerical reference simulation R0. Wind aligned with the y axis, free-slip bottom boundary condition.

in the main text) is presented. The horizontal dimensionless velocities u/U_0 and v/U_0 obtained from the complex solution (B.22) are plotted in Fig. B3 against the dimensionless depth ζ for the particular cases of latitude $\phi = 0°$ (Equator), $\phi = 45°, \phi = 90°$. As it was clear from the mathematical derivation, the proposed solution we derived is the same we obtain if we assume S1980. Such a solution perfectly fits the simulation outputs along x direction (u/U_0) and is different from the Ekman classic version when $\varepsilon > 0$ (Fig. B3c and e). Differently, along the wind direction y the longitudinal velocity v/U_0 from A2019 and S1980 solutions collapses onto the classic E1905 solution at all latitudes. In fact, it can be analytically demonstrated that in the solution proposed here (see Eq. (B.22)), the imaginary part of ω (i.e. $\omega_y = v/U_0$) is a function of the real value of σ only (σ_x), which is zero according to (B.23) if $\mathcal{T} = i$. Thus, for the case of free-slip boundary condition the classical solution proposed by Ekman for the along-wind velocity is equivalent to the one that takes into account the effect of pressure gradients. As ε increases, the matching between T2013 solution and the correct solution is lost: this was also found in the case of no-slip bottom boundary condition in the main text and can be ascribed to the increasing monotonic trend that the T2013 solution has due to its derivation with a perturbation method assuming small ε. This can be even more easily seen in Fig. B2 where crosswise transport is plotted in the case of free-slip boundary condition from numerical R0 outputs and analytical solutions. For $\varepsilon \leqslant 1$ the classical E1905 solution goes to infinity, while the proposed solution A2019 (which is equal to S1980) and T2013 provide the correct value for the transport. For $\varepsilon \geqslant 1$ the T2013 solution detaches from the numerical output and tends to infinity, while the E1905 well reproduces the correct trend in the right part of ε domain, where $\varepsilon \to \infty$ (See Fig. B4).

Appendix A. Supplementary data

Supplementary data associated with this article can be found, in the online version, athttps://doi.org/10.1016/j.jglr.2019.10.013.

References

Amadori, M., Piccolroaz, S., Giovannini, L., Zardi, D., Toffolon, M., 2018. Wind variability and Earth's rotation as drivers of transport in a deep, elongated subalpine lake: the case of Lake Garda. J. Limnol. 77 (3). https://doi.org/10.4081/jlimnol.2018.1814.

Antenucci, J.P., Imberger, J., 2001. Energetics of long internal gravity waves in large lakes. Limnol. Oceanogr. 46 (7), 1760–1773. https://doi.org/10.4319/lo.2001.46.7.1760.

Birchfield, G.E., 1972. Theoretical aspects of wind-driven currents in a sea or lake of variable depth with no horizontal mixing. J. Phys. Oceanogr. 2 (4), 355–362. https://doi.org/10.1175/1520-0485(1972)002<0355:TAOWDC>2.0.CO;2.

Boehrer, B., Schultze, M., 2008. Stratification of lakes. Rev. Geophys. 46 (2). https://doi.org/10.1029/2006RG000210.

Cheng, P., Valle-Levinson, A., 2009. Influence of lateral advection on residual currents in microtidal estuaries. J. Phys. Oceanogr. 39, 3177–3190.

Csanady, G.T., 1976. Mean circulation in shallow seas. J. Geophys. Res. 81 (30), 5389–5399. https://doi.org/10.1029/JC081i030p05389.

Csanady, G.T., 1982. Circulation in the Coastal Ocean. D. Reidel Pub..

Defant, A., 1962. Physical Oceanography Pergamon Press. London, 1961. Vol. 1, pp. xvi 729; Vol. 2, pp. viii 598, book review by J.B. Hersey. Journal of the Marine Biological Association of the United Kingdom 42(2), 468–468.https://doi.org/10.1017/S0025315400070089..

Dever, E.P., 1997. Wind-forced cross-shelf circulation on the Northern California shelf. J. Phys. Oceanogr. 27 (8), 1566–1580. https://doi.org/10.1175/1520-0485(1997) 027<1566:WFCSCO>2.0.CO;2.

Ekman, V.W., 1905. On the influence of the Earth's rotation on the ocean currents. Ark. Mat. Astr. Fys. 2 (11), 1–52.

Fjeldstad, J.E., 1930. Ein problem aus der windstromtheorie. J. Appl. Math. Mech. 10 (2), 121–137. https://doi.org/10.1002/zamm.19300100203.

Gedney, R.T., Lick, W., 1972. Wind-driven currents in Lake Erie. J. Geophys. Res. 77 (15), 2714–2723. https://doi.org/10.1029/JC077i015p02714.

Gill, A.E., 1982. Atmosphere-ocean dynamics, xv, 662 p. 189:214 pp. Academic Press. New York..

Griffiths, R.W., 1986. Gravity currents in rotating systems. Annu. Rev. Fluid Mech. 18 (1), 59–89. https://doi.org/10.1146/annurev.fl.18.010186.000423.

Heaps, N.S., 1984. Vertical structure of current in homogeneous and stratified waters. In: Hutter, K. (Ed.), Hydrodynamics of Lakes: CISM Lectures. Springer Verlag, pp. 153–207.

Heaps, N.S., Ramsbottom, A.E., 1966. Wind effects on the water in a narrow two-layered lake. Philos. Trans. R. Soc. London A 259 (1102), 391–430. https://doi.org/10.1098/rsta.1966.0021.

Hidaka, K., 1933. Non-stationary Ocean-currents. Mem. Imp. Mar. Obs. 3.

Hutter, C., Salvad, G., Spinedi, C., Zamboni, F., Bäuerle, E., 1991. Large scale water movements in lakes. Aquat. Sci. 53, 100–135. https://doi.org/10.1007/BF00877057.

Hutter, K., Wang, Y., Chubarenko, I.P., 2011. Physics of lakes. In: Volume 1: Foundation of the Mathematical and Physical Background, Advances in Geophysical and Environmental Mechanics and Mathematics. Springer.

Kasai, A., Hill, A.E., Fujiwara, T., Simpson, J.H., 2000. Effect of the Earth's rotation on the circulation in regions of freshwater influence. J. Geophys. Res.: Oceans 105 (C7), 16961–16969. https://doi.org/10.1029/2000JC900058.

Laborde, S., Antenucci, J.P., Copetti, D., Imberger, J., 2010. Inflow intrusions at multiple scales in a large temperate lake. Limnol. Oceanogr. 55 (3), 1301–1312. https://doi.org/10.4319/lo.2010.55.3.1301.

Lee, K.K., Ligget, J.A., 1970. Computation for circulation in stratified lakes. J. Hydraul. Div. 96 (10), 2089–2115.

Lesser, G.R., Roelvink, J.A., Keste, T.M.V., Stelling, G.S., 2004. Development and validation of a three-dimensional morphological model. Coast. Eng. 51, 883–915. https://doi.org/10.1016/j.coastaleng.2004.07.014.

Madsen, O.S., 1977. A realistic model of the wind-induced Ekman boundary layer. J. Phys. Oceanogr. 7 (2), 248–255. https://doi.org/10.1175/1520-0485(1977)007<0248:ARMOTW>2.0.CO;2.

Mohammed-Zaki, M.A., 1980. Time scales in wind-driven lake circulations. J. Geophys. Res.: Oceans 85 (C3), 1553–1562. https://doi.org/10.1029/JC085iC03p01553.

Okubo, A., 1971. Oceanic diffusion diagrams, Deep sea research and oceanographic abstracts 18(8), 789–802..

Piccolroaz, S., Toffolon, M., 2018. The fate of Lake Baikal: how climate change may alter deep ventilation in the largest lake on Earth. Clim. Change 150 (3), 181–194. https://doi.org/10.1007/s10584-018-2275-2.

Piccolroaz, S., Amadori, M., Dijkstra, M.T.H.A., 2019. Importance of planetary rotation for ventilation processes in deep elongated lakes: evidence from Lake Garda (Italy). Scientific Rep. 9. https://doi.org/10.1038/s41598-019-44730-1.

Pilotti, M., Valerio, G., Giardino, C., Bresciani, M., Chapra, S.C., 2018. Evidence from field measurements and satellite imaging of impact of Earth rotation on Lake Iseo chemistry. J. Great Lakes Res. 44 (1), 14–25. https://doi.org/10.1016/j.jglr.2017.10.005.

Platzman, G.W., 1963. The Dynamical Prediction of Wind Tides on Lake Erie. American Meteorological Society, Boston, MA, pp. 1–44.

Ponte, A., 2010. Periodic wind-driven circulation in an elongated and rotating basin. J. Phys. Oceanogr. 40, 2043–2058.

Ponte, A.L., Gutiérrez de Velasco, G., Valle-Levinson, A., Winters, K.B., Winant, C.D., 2012. Wind-driven subinertial circulation inside a semienclosed bay in the gulf of california. J. Phys. Oceanogr. 42 (6), 940–955. https://doi.org/10.1175/JPO-D-11-0103.1.

Rao, D.B., Murty, T.S., 1970. Calculation of the steady state wind-driven circulations in Lake Ontario. Archiv für Meteorol Geophys Bioklimatol Ser A 19 (2), 195–210. https://doi.org/10.1007/BF02249005.

Rossby, C.-G., 1937. On the mutual adjustment of pressure and velocity distributions in certain simple current systems I. J. Mar. Res. 1, 15–28.

Rossby, C.-G., 1938. On the mutual adjustment of pressure and velocity distributions in certain simple current systems II. J. Mar. Res. 1, 239–263.
Rueda, F.J., Vidal, J., 2009. In: Likens, G.E. (Ed.), Biogeochemistry of Inland Waters, pp. 286–300.
Sanay, R., Valle-Levinson, A., 2005. Wind-induced circulation in semienclosed homogeneous, rotating basins. J. Phys. Oceanogr. 35 (12), 2520–2531. https://doi.org/10.1175/JPO2831.1.
Schmid, M., Budnev, N.M., Granin, N.G., Sturm, M., Schurter, M., Wüest, A., 2008. Lake Baikal deepwater renewal mystery solved. Geophys. Res. Lett. 35 (9). https://doi.org/10.1029/2008GL033223.
Simons, T.J., 1980. Circulation models of lakes and inland seas, Canadian Bullettin of Fisheries and Aquatic Sciences. Bulletin 203, 146 pp. Department of Fisheries and Oceans..
Stocker, R., Imberger, J., 2003. Energy partitioning and horizontal dispersion in a stratified rotating lake. J. Phys. Oceanogr. 33 (3), 512–529. https://doi.org/10.1175/1520-0485(2003) 033<0512:EPAHDI>2.0.CO;2.
Svensson, U., 1979. The structure of the turbulent Ekman layer. Tellus 31 (4), 340–350. https://doi.org/10.3402/tellusa.v31i4.10442.
Thomas, J.H., 1975. A theory of steady wind-driven currents in shallow water with variable eddy viscosity. J. Phys. Oceanogr. 5 (1), 136–142. https://doi.org/10.1175/1520-0485(1975) 005<0136:ATOSWD>2.0.CO;2.
Toffolon, M., 2013. Ekman circulation and downwelling in narrow lakes. Adv. Water Resour. 53, 76–86. https://doi.org/10.1016/j.advwatres.2012.10.003.
Toffolon, M., Rizzi, G., 2009. Effects of spatial wind inhomogeneity and turbulence anisotropy on circulation in an elongated basin: a simplified analytical solution. Adv. Water Resour. 32, 1554–1566.
Tsimitri, C., Rockel, B., Wüest, A., Budnev, N.M., Sturm, M., Schmid, M., 2015. Drivers of deep-water renewal events observed over 13 years in the south basin of Lake Baikal. J. Geophys. Res.: Oceans 120 (3), 1508–1526. https://doi.org/10.1002/2014JC010449.
Valle-Levinson, A., 2008. Density-driven exchange flow in terms of the Kelvin and Ekman numbers. J. Geophys. Res.: Oceans 113 (C4). https://doi.org/10.1029/2007JC004144.
Valle-Levinson, A., Reyes, C., Sanay, R., 2003. Effects of bathymetry, friction, and rotation on estuary-ocean exchange. J. Phys. Oceanogr. 33 (2), 2375–2393.
Veronis, G., 1956. Partition of energy between geostrophic and non-geostrophic oceanic motions. Deep Sea Res. (1953) 3(3), 157–177.https://doi.org/10.1016/0146-6313(56)90001-6..
Wang, Y., Hutter, K., Bäuerle, E., 2001. Barotropic response in a lake to wind-forcing. Ann. Geophys. 19 (3), 367–388. https://doi.org/10.5194/angeo-19-367-2001.
Welander, P., 1957. Wind action on a shallow sea: some generalizations of Ekman's theory. Tellus 9 (1), 45–52. https://doi.org/10.1111/j.2153-3490.1957.tb01852.x.
Winant, C.D., 2004. Three-dimensional wind-driven flow in an elongated, rotating basin. J. Phys. Oceanogr. 34 (2), 462–476. https://doi.org/10.1175/1520-0485(2004) 034<0462:TWFIAE>2.0.CO;2.
Wüest, A., Lorke, A., 2003. Small scale hydrodynamics in lakes. Annu. Rev. Fluid Mech. 35, 373–412. https://doi.org/10.1146/annurev.fluid.35.101101.161220.